PAPER

High-temperature electrical capacitance tomography for gas–solid fluidised beds

IOP Publishing Measurement Science and Technology
Meas. Sci. Technol. **29** (2018) 104002 (10pp) https://doi.org/10.1088/1361-6501/aad641

High-temperature electrical capacitance tomography for gas–solid fluidised beds

Kai Huang[1,2], Shuanghe Meng[1], Qiang Guo[1,2], Mao Ye[1], Jingjing Shen[1,2], Tao Zhang[1], Wuqiang Yang[3] and Zhongmin Liu[1]

[1] Dalian National Laboratory for Clean Energy and National Engineering Laboratory for MTO, Dalian Institute of Chemical Physics, Chinese Academy of Sciences, Dalian 116023, People's Republic of China
[2] University of Chinese Academy of Sciences, Beijing 100049, People's Republic of China
[3] School of Electrical and Electronic Engineering, The University of Manchester, Manchester, M13 9PL, United Kingdom

E-mail: maoye@dicp.ac.cn

Received 30 March 2018, revised 11 July 2018
Accepted for publication 27 July 2018
Published 23 August 2018

Abstract

Electrical capacitance tomography (ECT) is a non-intrusive and non-invasive imaging technique for the visualisation of material distribution, e.g. in a gas–solid fluidised bed. So far, ECT has been successfully used in gas–solid fluidised beds at ambient temperature. However, ECT has been rarely used in high-temperature gas–solid fluidised beds, which is of practical importance in many applications. Considering that most fluidised bed reactors are operated at high temperature, it is necessary to investigate the application of ECT in high-temperature industrial processes. In this work, a high-temperature ECT sensor, which can withstand 1073 K, is designed and fabricated. It has been verified by three stationary objects. The results show that the ECT sensor can give satisfactory images at different high-temperature levels and the change in temperature has little effect on the signal-to-noise ratio. It has also been found that the minimum bubbling velocity estimated by ECT is the same as that obtained by pressure drop measurements, and two fluidisation regimes, i.e. bubbling and slugging can be identified by ECT.

Keywords: electrical capacitance tomography sensor, high temperature, fluidised bed, flow regime

(Some figures may appear in colour only in the online journal)

1. Introduction

Gas–solid fluidised beds are widely used in chemical and other industrial processes, such as fluid catalytic cracking, methanol-to-olefins and biomass gasification, because of their excellent mixing, heat transfer and continuous operation characteristics [1–3]. Because the performance of a gas–solid fluidised bed reactor depends on the interaction between the particles and gas, it is important to obtain information about the flow hydrodynamics of fluidised beds, such as the fluidisation regime, bubble diameter, solid distribution and solid flux. Different techniques have been used to measure the characteristics of fluidised beds, and they can be divided into invasive and non-invasive methods. Werther reviewed the invasive measurement methods, such as suction, capacitance and optical fibre probes [4], which are designed to measure the local information of fluidised beds with the limitation of altering the nearby flow structure. Non-invasive measurement methods are divided into tomography and velocimetry techniques according to Chaouki *et al* [5]. Tomography techniques are used to measure gas and solid distribution, while velocimetry techniques are used to measure fluid or particulate flow velocities in fluidised beds.

To date, measurement techniques to obtain the hydrodynamics of fluidised beds at high temperature have been very limited because of the opaqueness and harsh environment. Hence, most measurements are made at room temperature and then the results are extrapolated to a high temperature. Computational fluid dynamics is widely used to simulate the hydrodynamics of fluidised beds at high temperature.

However, the parameters used in the simulation are always derived from room-temperature results. Obviously, these parameters need to be verified by measurements at high temperature. Therefore, it is necessary to develop an experimental tool to obtain the hydrodynamics of fluidised beds at high temperature, so that the industrial operation involving high-temperature fluidised beds can be optimised by developing valid physical models of the fluidised beds.

Electrical capacitance tomography (ECT) is one of the non-intrusive and non-invasive techniques that has been widely applied to measure fluidisation regimes, bubble diameter, solid distribution and solid flux in circulating fluidised beds [6–9] because of its low cost, simple construction of ECT sensors and non-radioactive characteristics. Moreover, an ECT sensor has been used in flame measurement [10], indicating the possibility of using ECT in a high-temperature environment. There have been many reports in the literature regarding the visualisation of fluidised beds using tomography techniques [8, 11, 12] at room temperature, but very few involving high temperature. Velarde *et al* developed endoscopic-laser PIV/DIA equipment to investigate the hydrodynamics of a gas–solid fluidised bed at high temperature up to 723 K in a pseudo-2D fluidised bed [13] and concluded that high-temperature ePIV/DIA was a reliable technique to study the effect of temperature on the fluidisation characteristics of gas–solid fluidised beds. Recently, Ye *et al* designed an ECT sensor capable of withstanding high temperature for a fluidised bed reactor [14, 15]. Wang *et al* also extended their electrical capacitance volume tomography sensor to characterise gas–solid slugging fluidisation with Geldart group D particles under high temperature up to 923 K [16]. These findings indicate the feasibility of the application of a high-temperature ECT sensor for fluidised beds. However, the high-temperature ECT sensor was not quantitatively evaluated, in particular its performance against stationary objects and signal-to-noise ratio (SNR) at high temperature.

In this work, the developed high-temperature ECT sensor has been used in gas–solid fluidised beds up to 1073 K, and verified by stationary objects. The effect of temperature on the SNR is also studied. Based on the satisfactory performance of the ECT sensor, further investigation has been conducted on the high-temperature fluidised bed characteristics.

2. Experimental

2.1. Design of a high-temperature ECT sensor

A typical ECT system comprises three main units: sensor, sensing electronics and computer [17]. An ECT sensor consists of a set of capacitance electrodes mounted around a vessel and is used to measure the change in capacitance caused by the variation of relative permittivity or its distribution [17].

The high-temperature ECT sensor is developed [14, 15] following the work by Yang [18], and consists of eight measurement electrodes, two driven guard electrodes, two insulating frames, eight radial insulating stripes and two earthed screens. Figure 1(a) shows a cross-sectional view of the ECT sensor, which is designed for use in a 2 mm thick quartz fluidised bed with a 51 mm outer diameter. The length of the electrodes is 30 mm, the thickness of the electrodes is 2 mm and the gap between adjacent electrodes is 1 mm. Considering that the ECT sensor is used at high temperature, it is crucial to choose appropriate materials that can withstand high temperature and physical-chemical properties that are stable when the temperature changes. The measurement electrodes are made of stainless steel with a connector, as shown in figure 1(b). A photo and sketch map of the high-temperature ECT sensor mounted on a fluidised bed column is shown in figure 2. There are a number of differences between this high-temperature ECT sensor and room-temperature ECT sensors:

(1) Two earthed screens are used. The interior earthed screen made of aluminium foil 0.5 mm thick is used to fasten the electrodes and reduce external noise.
(2) The coaxial cables are specially designed with stainless-steel wires, enclosed by a hollow ceramic tube. The outer covering is a shielding net that can withstand high temperature. The high-temperature coaxial cables are extended to the outside of the furnace and connected with normal cables.
(3) Two driven guard electrodes made of 0.5 mm thick stainless steel are used to reduce noise.
(4) A quartz band is used to insulate the electrodes and interior earthed screen in addition to fastening the electrodes. Another quartz band is used between the interior and exterior earthed screen to fasten the exterior earthed screen to the ECT sensor body.

2.2. Fluidised bed set-up and experiment procedure

As shown in figure 2, the fluidised bed is made of a 1 m length of 2 mm thick quartz with an outer diameter of 51 mm. The distribution plate is made by calcining around 200 μm mean diameter quartz sand and the thickness of the plate is 10 mm. The ECT sensor is located at 185 mm above the distribution plate. Dry compressed air is used for fluidisation. A mass flowmeter with a measurement range up to 5 l min^{-1} is used to control the air and the air velocity is calibrated by an ideal gas equation at the set temperature. The length of the chamber is set to 300 mm to make air reach the set temperature, which is measured by a thermocouple. The whole fluidised bed is heated by a two-section tubular furnace. A differential pressure transducer is used to measure the pressure drop of the whole fluidised bed. The differential pressure of the distribution plate is measured and subtracted after the experiment where the differential pressure of the fluidised bed is obtained. The measurement range of the differential pressure is 5000 Pa and its accuracy is 0.25% of the full scale. The sampling frequency is set at 115 Hz, which is the data acquisition rate of the ECT system and the sampling number is 1000 for each experiment. Solid–gas two-phase flow in the fluidized bed is indeed highly dynamic, which is mainly caused by the dynamics of the gas bubbles including frequent bubble formation, coalescence and eruption in the dense bed. It has been widely found [19–23] that the dominant frequency of bubble dynamics is typically below 10 Hz in fluidized beds and

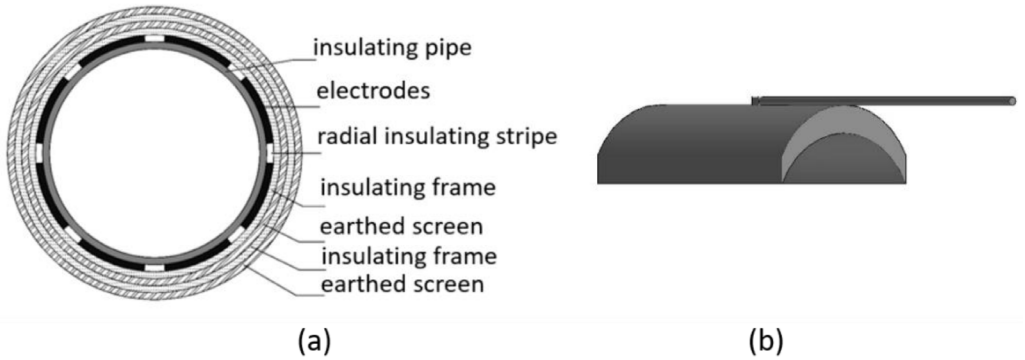

Figure 1. Construction of the high-temperature ECT sensor. (a) Cross-sectional view of the designed ECT sensor. (b) Electrode with connector.

average solid concentration is a direct representative of bubble behaviour in the fluidized bed, so the dominant frequency is typically below 10 Hz. Normally, the average solid concentration time series is treated by fast Fourier transformation to get the dominant frequency. According to Shannon's sampling theorem, frequencies below half the acquisition frequency, i.e. 57.5 Hz in our experiments, can be accurately obtained. So, the acquisition frequency to 115 Hz is satisfactory to get the dominant frequency in this work.

Activated alumina particles with a Sauter diameter of 90 μm and density of 1500 kg m^{-3} are used at the test temperature. The particles are first calcinated at 873 K for 5 h to stabilise the chemical and physical properties and then stored in a desiccator.

An AC-based ECT system is used to measure the capacitance from the ECT sensor [24]. It needs to be calibrated in advance. The fluidised bed is first heated to a set temperature and calibrated with low-permittivity material (i.e. air), and then by activated alumina. The fluidised bed is kept at the minimum fluidisation state for 1 h to eliminate moisture and kept in the packed bed state for 30 min before the ECT system is calibrated with high-permittivity material (i.e. activated alumina). After calibration, measurements are conducted at 293, 473, 673, 873 and 1073 K with several fluidised velocities.

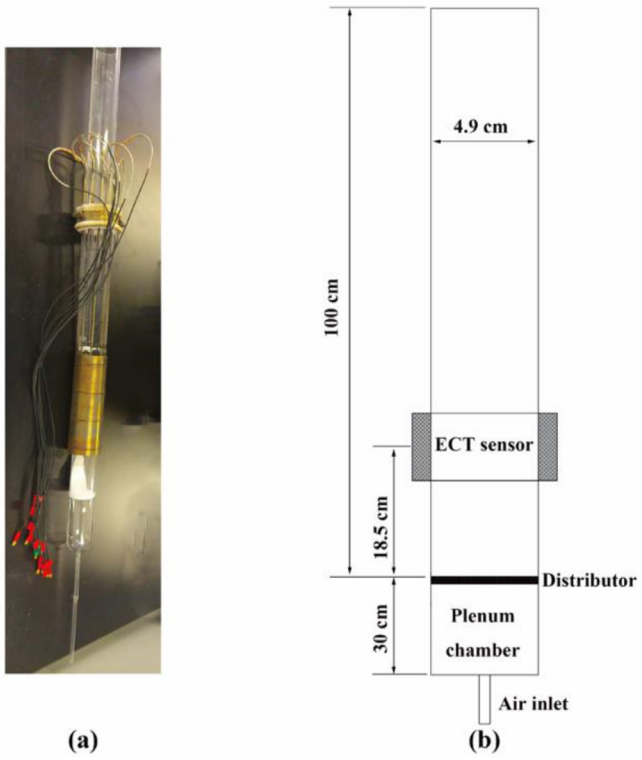

Figure 2. High-temperature ECT sensor mounted in a fluidised bed column. (a) Photo. (b) Location of the ECT sensor in the fluidised bed.

3. Data analysis methods

3.1. Image reconstruction

3.1.1. The effect of temperature. An ECT sensor with different pairs of electrodes basically detects the change of capacitance between each electrode pair around a fluidised bed column, which is a function of the media permittivity of the sampling regime inside the fluidised bed. The media permittivity distribution is in fact dependent on the material distribution, i.e. solid concentration distribution and temperature. The variation of solid concentration distribution and temperature would virtually alter the capacitance detected by the ECT sensor. Thus, we can obtain:

$$C = f(g, T), \tag{1}$$

where g is the solid concentration distribution and T is temperature distribution. The change in capacitance in response to the perturbations of solid concentration and temperature is given by:

$$\Delta \mathrm{C} = \frac{\partial f}{\partial g}\Delta g + \frac{\partial f}{\partial T}\Delta T + O\left((\Delta g)^2\right) + O\left((\Delta T)^2\right), \tag{2}$$

where $\frac{\partial f}{\partial g}$ is the sensitivity of the capacitance to solid concentration distribution and $\frac{\partial f}{\partial T}$ is the sensitivity of the capacitance to the temperature. Note that $O\left((\Delta g)^2\right)$ and $O\left((\Delta T)^2\right)$ respectively represent the higher-order terms $(\Delta g)^2$ and $(\Delta T)^2$, which can be ignored when the perturbations of solid concentration and temperature are sufficiently small. When ECT is used to measure the fluidised bed at ambient temperature, the variation in temperature is negligible and equation (2) is reduced to

$$\Delta C = \frac{\partial f}{\partial g}\Delta g. \tag{3}$$

Equation (3) can be simplified to the linear form

$$\Delta C = s\Delta g, \tag{4}$$

where $s = \frac{\partial f}{\partial g}$ is the sensitivity of the capacitance to solid concentration and this formula is the basis of ECT applications at ambient temperature. But, when the influence of the temperature on the permittivity cannot be neglected, equation (3) can be simplified to the linear form

$$\Delta C = s\Delta g + k\Delta T, \tag{5}$$

where $k = \frac{\partial f}{\partial T}$ is the sensitivity of the capacitance to the changes in temperature. Equation (5) can be further rewritten as

$$\Delta C - k\Delta T = s\Delta g. \tag{6}$$

The comparison between equations (4) and (6) shows that correction to the measured capacitances has to be made before the reconstruction algorithms can be used. However, the derivation of the sensitivity k is extremely hard as the relation between material permittivity and temperature can vary to a large extent. In this work, fortunately, the rapid back-mixing of particles in the fluidised bed leads to the uniform distribution of temperature in the dense bed. The measurement of temperature at different locations in the fluidised bed studied in this work indicated that the maximum temperature difference of 35 K could be achieved in extreme cases (i.e. the bed is packed at a velocity lower than the minimum fluidisation velocity). Such a narrow temperature difference significantly reduces the influence of the temperature on the permittivity in the ECT measurements performed in this work [25]. Another challenge is the influence of the temperature gradient of the wall of the fluidised bed column. The temperature difference across the wall of a hot fluidised bed is normally very large. If the ECT sensor is attached to the outer wall of the fluidised bed, the large temperature variation across the wall might cause significant change of the permittivity. According to Wang *et al* [25], the relative permittivity change of quartz with temperature from 293–1273 K is only 10^{-4}/K, which on the one hand shows very good thermal stability and on the other hand suggests that for the fluidised bed made of quartz the large temperature variation across the wall only has a minor effect on the measurement. Actually, in this work, our main purpose is to test the reliability of our ECT sensor used under high temperature. In a parallel work, a theoretical work considering the effect of temperature together with experimental validation in a reactor with a large temperature gradient is being undertaken by our group, and it is the subject of another publication.

3.1.2. Image reconstruction algorithm. With the eight-electrode ECT sensor, 28 independent capacitance measurements are obtained and used to reconstruct an image with 64 × 64 pixels. As reported by Yang and Peng [26], a satisfactory image is obtained using the projected Landweber iteration algorithm as follows:

$$\widehat{g_0} = S^T\lambda \tag{7}$$

$$\widehat{g_{k+1}} = P\left[\widehat{g_k} - \alpha S^T\left(S\widehat{g_k} - \lambda\right)\right],$$

$$P[f(x)] = \begin{cases} 0 & \text{if } f(x) < 0 \\ f(x) & \text{if } 0 \leqslant f(x) \leqslant 1 \\ 1 & \text{if } f(x) > 1 \end{cases}, \tag{8}$$

where g is a vector indicating the normalised permittivity distribution, i.e. the reconstructed grey level in each image pixel, S is the normalised sensitivity matrix, α is the step length and set at 1.2 in this work, k is the iteration step, and λ is a normalised capacitance vector, which is defined as

$$\lambda_{ij} = \frac{C_{ij}^m - C_{ij}^l}{C_{ij}^h - C_{ij}^l}, \tag{9}$$

where C_{ij}^m is the measured capacitance of the *i–j* electrode pair, C_{ij}^l and C_{ij}^h are the capacitances measured with an empty and packed bed of the *i–j* electrode pair, which are obtained during the system calibration.

A sensitivity matrix is commonly obtained using [27]

$$S_{ij}^*(x,y) = \int_{P(x,y)} \frac{E_i(x,y)}{V_i} \cdot \frac{E_j(x,y)}{V_j} \mathrm{d}x\mathrm{d}y. \tag{10}$$

A normalised sensitivity matrix S is calculated as

$$S_{mn} = \frac{S_{mn}^*}{\sum_{n=1}^{N} S_{mn}^*}, \tag{11}$$

where S_{mn} and S_{mn}^* are entries in the mth row and nth column of S and S^*, respectively, and N is the effective number of pixels in the image area, which is 3228 in a 64 × 64 pixel structure.

Note that in principle the sensitivity matrix should change with the permittivity distribution. However, a generic sensitivity matrix S, which is calculated based on a vacuum permittivity distribution [15, 28], is commonly used to reconstruct images. It should also be noted that the relative permittivity of the wall varies with temperature, and hence the sensitivity matrix needs to be validated at different temperatures by simulation. Wang *et al* [29] found the variation rate of relative permittivity of quartz sand with temperature is only 10^{-4}/K. The relative permittivity of the quartz fluidised bed wall changes around 0.058 from 293 to 873 K and the relative change is only 1.5%. Such a small change in relative permittivity of the wall has little effect on image reconstruction. Therefore, the generic sensitivity matrix obtained at room temperature is used to reconstruct images in this work. The normalised permittivity distribution is regarded as the relative solid concentration.

3.2. Average solid concentration

The solid concentration is calculated by averaging the normalised permittivity of image pixels, i.e. 3228 pixels in a

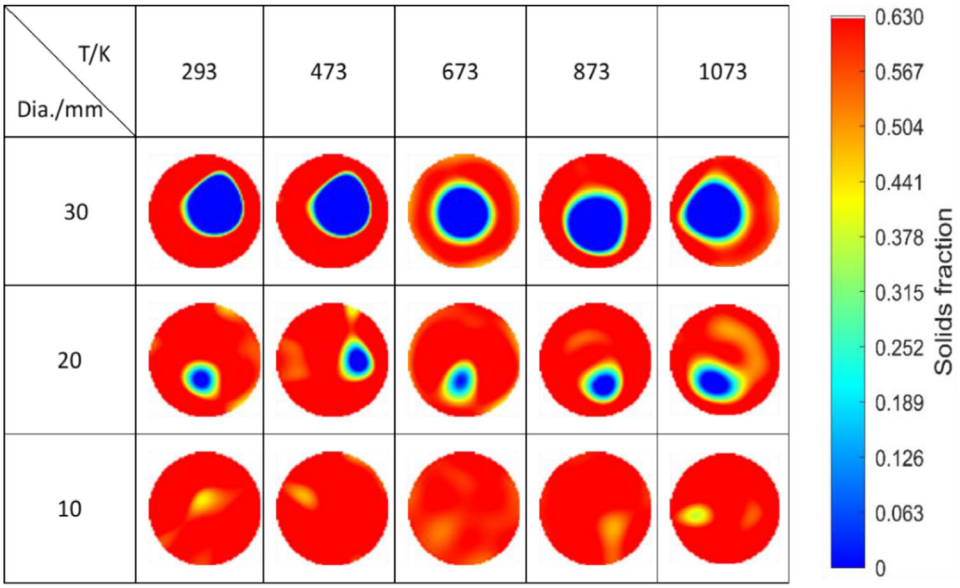

Figure 3. Images of quartz tubes inserted into the fluidised bed at the packed state at different temperatures.

64 × 64 pixel structure, and multiplying the solid concentration of the packed bed as given in equation (12), where β is the solid concentration of one frame, S is the area of each image pixel and θ is the solid concentration of the packed bed, which is set to be 0.63. The average solid concentration is calculated by equation (13), where P is the frame of one measurement, i.e. 1000 in this work.

$$\beta = \theta \cdot \widehat{g} = \theta \cdot \frac{\sum_{i=1}^{N} g_i * s_i}{\sum_{i=1}^{N} s_i} \tag{12}$$

$$\overline{\beta} = \frac{1}{P}\sum_{i=1}^{P} \beta_i. \tag{13}$$

3.3. SNR

Image reconstruction using measured normalised capacitances with the generic sensitivity matrix is an ill-posed and ill-conditioned problem. Therefore, the SNR of the obtained signal is important for reconstructing images. Ye *et al* [30] used the following definition for the SNR:

$$S_{\mathrm{NR}} = 20\log_{10}\sqrt{\frac{\sum_{i=1}^{P} C_{mi}^2}{\sum_{i=1}^{P}\left(C_{mi} - \overline{C_m}\right)^2}} \tag{14}$$

$$\overline{S_{\mathrm{NR}}} = \sum_{i=1}^{M} S_{\mathrm{NR}(i)}/M \tag{15}$$

where C_{mi} is the measured relative capacitance of i frame from an electrode pair, $\overline{C_m}$ is the average normalised capacitance of one steady measurement of one electrode pair, P is the measurement frame number of one steady measurement, i.e. 1000 frame measurements, $\overline{S_{\mathrm{NR}}}$ is the average SNR of all electrode pairs and M is the number of all electrode pairs, i.e. 28 in this work.

4. Results and discussions

To verify the performance of the developed ECT sensor under high temperature, experiments were carried out at 293, 473, 673, 873 and 1073 K. This section covers the verification of the ECT measurements at test temperature using different methods, followed by the identification of the fluidisation regimes of Geldart A particles at high temperature by ECT measurements.

4.1. Imaging stationary objects

The three tested quartz tubes (35, 20 and 10 mm in outer diameter) with a sealed bottom were used to evaluate the performance of the developed sensor under high temperature. The thickness of the tube wall is 2 mm. Although materials with different dielectric properties can be added to the tubes, in the current work no other materials have been used, and the tubes are empty and filled with air. This is because the permittivity of air is not sensitive to the change of temperature, and we can compare the performance of the sensor for different tube sizes under high temperature. In the measurements, gas velocity was first set to three times the minimum bubbling velocity to make the bed fully fluidised, and the tubes were carefully inserted from the top of the column to the dense fluidised bed and mounted to the column. Then, the gas velocity was reduced gradually to zero to form a packed bed, which was kept for 30 min before we started the measurements in the packed bed regime. After all the measurements in the packed bed regime were completed, we set the superficial gas velocity to the targeted velocities (between one and 20 times the minimum bubbling velocities), kept the fluidised bed for a certain time until the temperature became stable, and then performed the measurement in the fluidised bed regime. Both packed and fluidised bed situations were tested. Shown in figure 3, are the images of two tubes 35 and 20 mm in diameter that agree with real situations at all test temperatures with

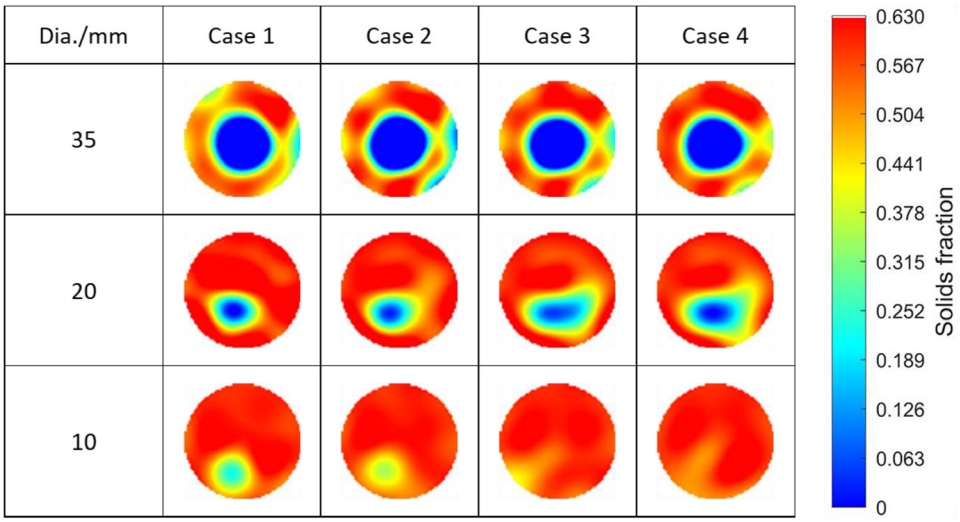

Figure 4. Images of quartz tubes inserted into the fluidised bed operated at a gas velocity of 4.67 cm s^{-1} and temperature of 873 K.

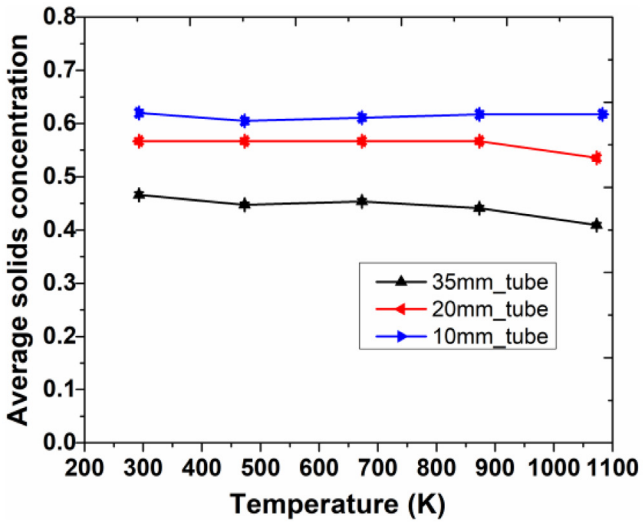

Figure 5. Average solid concentration of the cross-section of fluidised bed column, corresponding to the cases shown in figure 3.

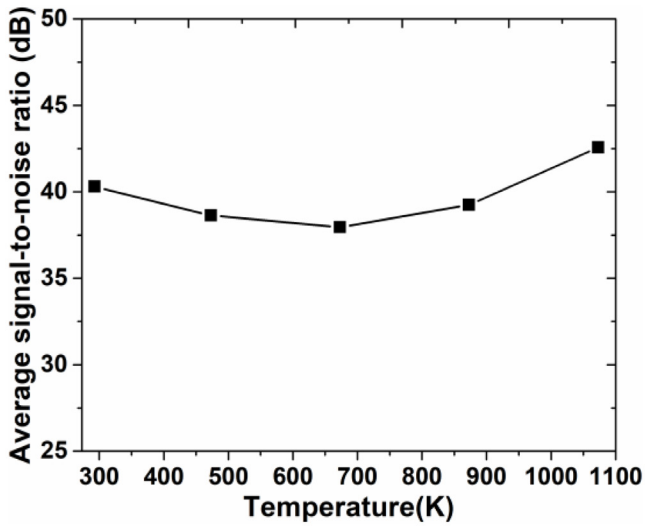

Figure 6. Variation of the SNR of the average solid concentration of the cross-section of the fluidised bed column, corresponding to the cases with quartz tube size of 35 mm shown in figure 3.

a packed bed. The image of the 10 mm diameter tube is similar to the real situation, but does not coincide with real images for all test temperatures, because of the low image resolution of ECT. Images are also obtained under fluidisation, as shown in figure 4, and the four cases are four randomly chosen moments from the experiments at a temperature of 873 K and superficial gas velocity of 4.67 cm s^{-1}, which further confirms the performance of the ECT sensor.

In the experiments, quartz tubes with different sizes were used to simulate gas bubbles in the fluidized bed, and the average solid concentration reported here was measured by the ECT sensor attached to the outside wall of the reactor. Thus, the average solid fraction is actually averaged over the cross-section of the reactor, which includes the area occupied by the empty tubes. As the solid concentration of the packed bed surrounding the empty tube almost remains unchanged, the average solid concentration over the cross-section of the reactor will be directly related to the size of the empty tube.

Figure 5 shows the variation of average solid concentration with temperature when empty tubes with outer diameters of 10, 20 and 35 mm, respectively, were inserted into the packed bed, and the SNR for the empty tube with a diameter of 35 mm at different temperatures was compared in figure 6. As can be seen, both the average solid concentration and corresponding SNR at different temperatures are consistent for the same tube size, which suggests that the sensor developed in this work can work well at temperatures up to 1073 K.

4.2. Minimum bubbling velocity

Measurement of the minimum fluidisation velocity using ECT was reported by some researchers [21, 22]. In their studies, Geldart B particles were used, and they obtained the minimum bubbling velocity equal to the minimum fluidisation velocity. In this work, Geldart A particles were used, and the minimum

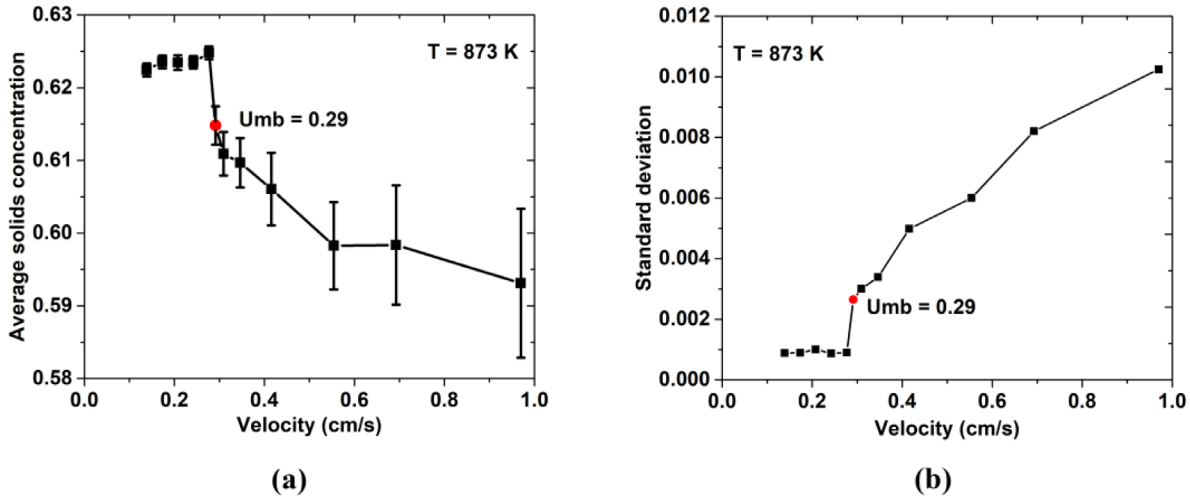

Figure 7. Average solid concentration and corresponding standard deviation as a function of the superficial gas velocity at a temperature of 873 K. (a) Average solid concentration against velocity. (b) Standard deviation against velocity.

bubbling velocity was obtained. The minimum bubbling velocity obtained by two ECT methods at 873 K were used to validate the performance of the developed sensor. First, the variation of average solid concentration with the superficial velocity is used to verify the minimum bubbling velocity, as shown in figure 7(a). It can be seen that a dramatic decrease happens at gas velocity $u_g = 0.29\,\text{cm s}^{-1}$. As the relatively small interval of $0.01\,\text{cm s}^{-1}$ was used in this experiment, we considered this point as the minimum bubbling fluidisation point, which was further confirmed by the snapshots shown in figure 8(b).

Another way to verify the minimum bubbling velocity is by checking the variation of the standard deviation of the average solid concentration against the superficial velocity. This method is similar to the use of the average solid concentration to verify the minimum bubbling velocity and the result is shown in figure 7(b). It can be established that the minimum bubbling velocity is $0.29\,\text{cm s}^{-1}$. When using the two methods, the same results were obtained, which was confirmed by visual observation and ECT images, as shown in figure 8(b). Pressure drop measurement across the whole bed is also used to verify the minimum bubbling velocity [31]. In the experiments with the air velocity step-by-step increasing, the minimum bubbling velocity (u_{mb}) is taken at the point where a shallow minimum of pressure drop (Δp) against superficial velocity (u) curve occurs, as shown in figure 8(a). The minimum bubbling velocity $u_{mb} = 0.29\,\text{cm s}^{-1}$, and the results are in good agreement with the ECT measurements. Figure 8(b) shows images by ECT measurement at the packed ($0.28\,\text{cm s}^{-1}$) and minimum bubbling state ($0.29\,\text{cm s}^{-1}$), which clearly reveals transition to the bubbling fluidisation regime. The minimum fluidisation velocity (U_{mf}) of the particles at 873 K is $0.27\,\text{cm s}^{-1}$ by the de-fluidising method, as shown in figure 8(a). The interval between the minimum fluidisation velocity and minimum bubbling velocity shows particulate fluidisation at 873 K.

4.3. Transition from bubbling to slugging fluidisation

In the previous section, the high-temperature ECT sensor was validated. In the following, the identification of fluidisation regimes for Geldart A particles at high temperature was conducted. The identification of fluidisation regimes by ECT was reported by Makkawi and Wright [22]. In their work, a time series of average solid concentration at different velocities was used to identify fluidisation regimes, which were analysed in frequency and temporal domains. They classified the fluidisation regimes as bubbling, slugging, turbulent and fast fluidisation. In industry, fluidised beds are often operated at high temperature. Therefore, it is important to identify the fluidisation regime by a simple and suitable way at high temperature.

The hydrodynamics in the bubbling fluidisation regime is mainly related to the bubbling dynamics in the fluidised bed [19, 20, 23]. In our relatively small fluidised bed apparatus, the bubbling fluidisation can be easily developed into slugging fluidisation, and the fluctuation of average solid concentration in time and frequency domain can reflect the fluidisation regime transition according to Makkawi and Wright [22]. Therefore, in this work, we also analysed the fluctuation of average solid concentration in time and frequency domain and tried to infer such a fluidisation regime transition under high temperature by use of the developed ECT sensor. A pressure drop time series was also used for comparison.

Figure 9(a) shows the variation of average solid concentration against velocity at 873 K. Regime transition by different slopes was clearly seen. Two regimes are identified: (1) bubbling regime for a velocity range between $U_{mb} = 0.29\,\text{cm s}^{-1}$ and $U_s \sim 1.1\,\text{cm s}^{-1}$, ($U_s$ is the superficial velocity at the transition to the slugging regime), and (2) slugging regime for a velocity greater than U_s at 873 K, as shown in figure 9(a). The bubbling regime is defined as the velocity between the minimum bubbling velocity (U_{mb}) and transition velocity (U_s). In this regime, small bubbles are formed, but cannot be visualised separately by ECT and the fluidised bed surface does

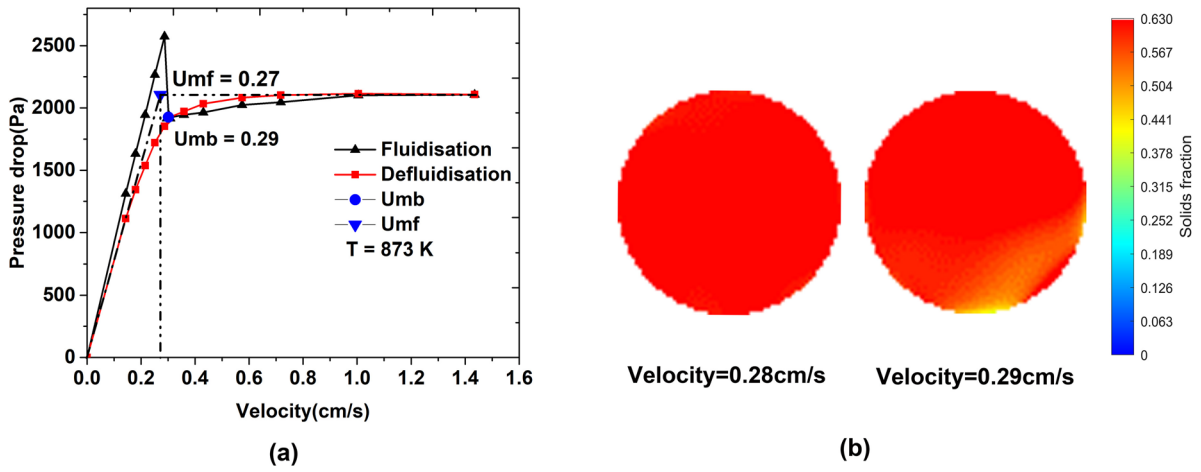

Figure 8. Pressure drop against velocity and images at different velocities. (a) Pressure drop against velocity. (b) Images from ECT measurements at different velocities.

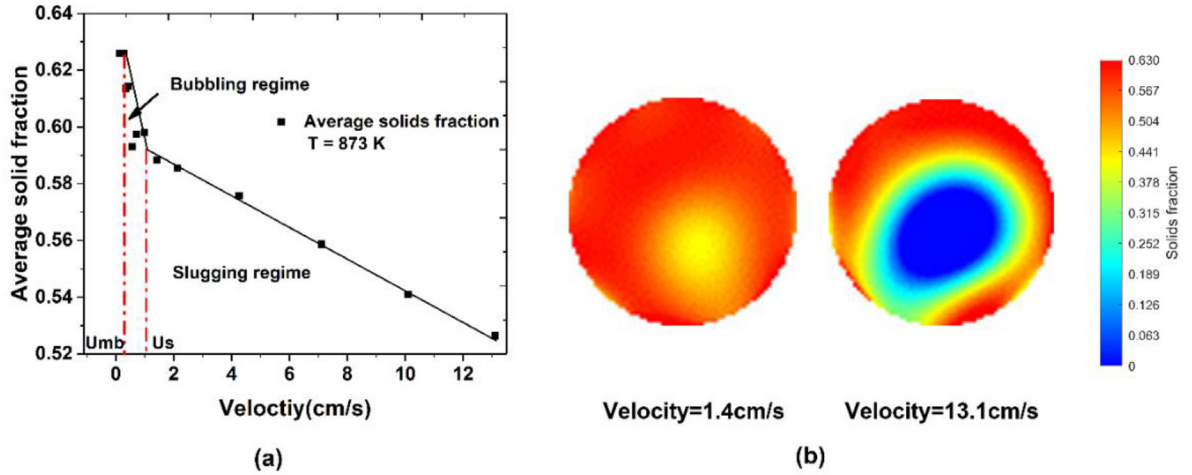

Figure 9. Average solid concentration against velocity and images in the slugging regime. (a) Average solid concentration against velocity. (b) Images from ECT measurements in the slugging regime.

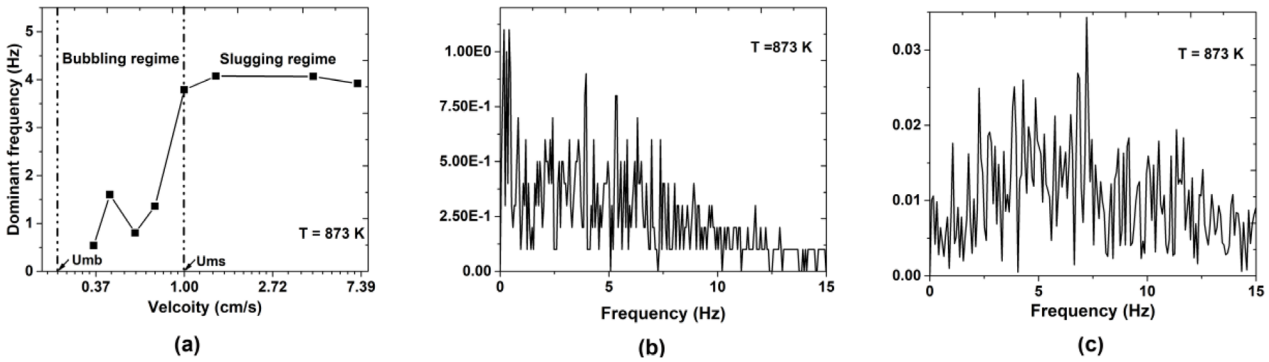

Figure 10. Dominant frequency with velocity and frequency spectrogram at different fluidization regimes. (a) Dominant frequency with velocity. (b) Frequency spectrogram in bubbling regime, velocity $= 0.42\,\mathrm{cm\ s^{-1}}$. (c) Frequency spectrogram in slugging regime, velocity $= 13.1\,\mathrm{cm\ s^{-1}}$.

not fluctuate strongly. The slugging regime is defined as the bubble diameter larger than half of the fluidised bed diameter and can be visualised by ECT, as shown in figure 9(b). In this regime, strong fluctuation of the fluidised bed surface can be seen by visual observation and the bubble diameter is increasing gradually with velocity.

In addition, dominant frequency analysis can be used to validate different fluidisation regimes [22]. A fast Fourier

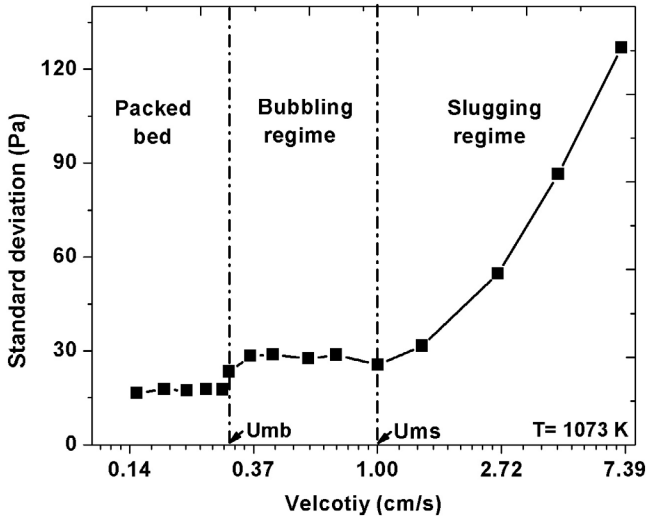

Figure 11. Standard deviation of pressure drop against superficial velocity.

transform algorithm is used to treat the average solid concentration time series and obtain the frequency spectrogram of the average solid concentration. The frequency, which has the maximum module, is regarded as the dominant frequency. In figure 10(a), six sets of experimental data were averaged and analysed. The typical frequency spectrogram in the bubbling and slugging regime is shown in figures 10(b) and (c), respectively. As can be seen, a notable transition between the bubbling regime and slugging regime can be identified at 1.00 cm s^{-1}. In the bubbling regime, small bubbles irregularly formed and erupted, inducing a noisy yet small dominant frequency (less than 1.5 Hz in our experiments). In the slugging regime, large slugs with equivalent size larger than 50% of the diameter of the column formed and erupted on a regular basis and thus a stable dominant frequency of around 4 Hz is obtained. Thus, we marked the regime between the minimum bubbling velocity and this transition velocity as the bubbling regime, and the regime beyond this transition velocity as the slugging regime. In experiments, as shown in figure 10(a), the dominant frequency increases remarkably from below 1.5 to around 4.00 Hz during the transition from bubbling fluidisation to slugging fluidisation.

As the pressure drop fluctuation is often used to distinguish the flow regime transition in the fluidised bed, we measured the pressure drop at different gas velocity and showed the average standard deviation of the pressure drop series in figure 11. As can be seen, there are two plateaus before the standard deviation of the pressure drop starts to increase dramatically at 1.00 cm s^{-1}. The first plateau is below the gas velocity of 0.30 cm s^{-1} and the second is between 0.30 and 1.00 cm s^{-1}, which indicates that the minimum bubbling velocity and transition velocity to slugging fluidisation are 0.30 and 1.00 cm s^{-1}, respectively. These results are consistent with the ECT measurements, as discussed above. Apparently, the bubbling and slugging fluidisation regimes can be clearly identified. Further work will be carried out to investigate the effect of temperature on fluidisation regime transition for particles of different Geldart groups.

5. Conclusions

In this work, for the first time, we demonstrate the evaluation of our invented sensor in high-temperature fluidized bed measurements up to 1073 K. First, static ECT images of quartz tubes with different sizes in a packed bed were measured, and the average solid concentration derived from the reconstructed images show that the performance of the ECT sensor is satisfactory at high temperature. Then, the minimum bubbling velocity at different temperatures was analysed by high-temperature ECT and compared with the pressure drop measurement, showing good agreement. Also, the transition of bubbling fluidization to slugging fluidization was analysed based on the frequency analysis of the average solid concentration time series. The results were also compared to the fluctuation of pressure drop and showed that the transition point predicted by the ECT images and pressure drop signal is consistent. The developed ECT sensor, which can withstand temperature up to 1073 K, is potentially a powerful tool for characterising fluidisation at high temperature.

Yet, the reconstruction algorithm and some other aspects used in this work share similarity with ECT measurements under ambient conditions, since this evaluation is carried out in a fluidized bed operated at a lower gas velocity, in which the temperature gradient is very small and the effect of temperature on permittivity can be ignored. But it is not our objective to complete all the theoretical and experimental aspects for the high-temperature ECT sensor in this contribution. In a parallel work, an ECT theoretical work considering the effect of temperature together with experimental validation in a reactor with a large temperature gradient is being undertaken by our group, and is the subject of another publication.

Acknowledgments

This work is financially supported by the Newton Advanced Fellowship of the Royal Society, UK, under Grant No. NA140308 and the National Key Research and Development Program of China (Grant No. 2018YFB0604904).

ORCID iDs

Kai Huang https://orcid.org/0000-0002-9024-0643
Qiang Guo https://orcid.org/0000-0002-8857-1961
Mao Ye https://orcid.org/0000-0002-7078-2402

References

[1] Grace J R 2016 Fluidised-bed catalytic reactors *Multiphase Catalytic Reactors: Theory, Design, Manufacturing, and Applications* (New York: Wiley)
[2] Tian P, Wei Y, Ye M and Liu Z 2015 Methanol to olefins (MTO): from fundamentals to commercialization *ACS Catal.* **5** 1922–38
[3] Wei G, He F, Zhao Z, Huang Z, Zheng A, Zhao K and Li H 2015 Performance of Fe–Ni bimetallic oxygen carriers for chemical looping gasification of biomass in a 10 kWth

interconnected circulating fluidised bed reactor *Int. J. Hydrog. Energy* **40** 16021–32
[4] Werther J 1999 Measurement techniques in fluidised beds *Powder Technol.* **102** 15–36
[5] Chaouki J, Larachi F and Duduković M P 1997 Noninvasive tomographic and velocimetric monitoring of multiphase flows *Ind. Eng. Chem. Res.* **36** 4476–503
[6] Chandrasekera T C, Li Y, Moody D, Schnellmann M A, Dennis J S and Holland D J 2015 Measurement of bubble sizes in fluidised beds using electrical capacitance tomography *Chem. Eng. Sci.* **126** 679–87
[7] Zhao T and Takei M 2010 Discussion of the solids distribution behavior in a downer with new designed distributor based on concentration images obtained by electrical capacitance tomography *Powder Technol.* **198** 120–30
[8] Liu S, Chen Q, Wang H G, Jiang F, Ismail I and Yang W Q 2005 Electrical capacitance tomography for gas–solids flow measurement for circulating fluidised beds *Flow Meas. Instrum.* **16** 135–44
[9] Guo Q, Meng S, Zhao Y, Ma L, Wang D, Ye M and Liu Z 2018 Experimental verification of solid-like and fluid-like states in the homogeneous fluidisation regime of Geldart A particles *Ind. Eng. Chem. Res.* **57** 2670–86
[10] He R, Xie C G, Waterfall R C, Beck M S and Beck C M 1994 Engine flame imaging using electrical capacitance tomography *Electron. Lett.* **30** 559–60
[11] Verma V, Padding J T, Deen N G, Kuipers J A M, Barthel F, Bieberle M and Hampel U 2014 Bubble dynamics in a 3D gas-solids fluidised bed using ultrafast electron beam x-ray tomography and two-fluid model *AIChE J.* **60** 1632–44
[12] Babaei R, Bonakdarpour B and Ein-Mozaffari F 2015 The use of electrical resistance tomography for the characterization of gas holdup inside a bubble column bioreactor containing activated sludge *Chem. Eng. J.* **268** 260–9
[13] Velarde I C, Gallucci F and van Sint Annaland M 2016 Development of an endoscopic-laser PIV/DIA technique for high-temperature gas–solid fluidised beds *Chem. Eng. Sci.* **143** 351–63
[14] Ye M, Luo Q, Meng S, Zhang T and Liu Z 2015 An electrical capacitance tomography sensor withstanding high temperature and its fabrication method *Chinese Patent*, CN 106556629A (in Chinese)
[15] Ye M, Guo Q, Meng S, Zhang T and Liu Z 2015 An electrical capacitance tomography sensor withstanding high temperature *Chinese Patent*, CN 106896143A (in Chinese)
[16] Wang D, Xu M, Marashdeh Q, Straiton B, Tong A and Fan L S 2018 Electrical capacitance volume tomography for characterization of gas–solid slugging fluidisation with Geldart group D particles under high temperatures *Ind. Eng. Chem. Res.* **57** 2687–97
[17] Xue Q, Wang H, Cui Z and Yang C 2012 Electrical capacitance tomography using an accelerated proximal gradient algorithm *Rev. Sci. Instrum.* **83** 043704
[18] Yang W 2010 Design of electrical capacitance tomography sensors *Meas. Sci. Technol.* **21** 042001
[19] Sasic S, Bo L and Johnsson F 2007 Characterization of fluid dynamics of fluidized beds by analysis of pressure fluctuations *Prog. Energy Combust. Sci.* **33** 453–96
[20] Bi H T 2007 A critical review of the complex pressure fluctuation phenomenon in gas–solids fluidized beds *Chem. Eng. Sci.* **62** 3473–93
[21] Li X, Jaworski A J and Mao X 2017 Comparative study of two non-intrusive measurement methods for bubbling gas-solids fluidised beds: electrical capacitance tomography and pressure fluctuations *Flow Meas. Instrum.* accepted (https://doi.org/10.1016/j.flowmeasinst.2017.08.002)
[22] Makkawi Y T and Wright P C 2002 Fluidisation regimes in a conventional fluidised bed characterised by means of electrical capacitance tomography *Chem. Eng. Sci.* **57** 2411–37
[23] Johnsson F, Zijerveld R C, Schouten J C and Leckner B 2000 Characterization of fluidization regimes by time-series analysis of pressure fluctuations *Int. J. Multiph. Flow* **26** 663–715
[24] Yang W and York T 1999 A new AC-based capacitance tomography system *IEEE Proc. Sci. Meas. Technol.* **146** 47–53
[25] Auerkari P 1996 Mechanical and physical properties of engineering alumina ceramics *Espoo: Technical Research Centre of Finland Report* pp 6–24
[26] Yang W and Peng L 2003 Image reconstruction algorithms for electrical capacitance tomography *Meas. Sci. Technol.* **14** R1–13
[27] Mou C H, Peng L H, Yao D Y, Zhang B and Xiao D Y 2006 A calculation method of sensitivity distribution with electrical capacitance tomography *Chin. J. Comput. Phys.* **1** 87–92
[28] Guo Q, Meng S, Wang D, Zhao Y, Ye M, Yang W and Liu Z 2018 Investigation of gas-solids bubbling fluidised beds using ECT with a modified Tikhonov regularization technique *AIChE J.* **64** 29–41
[29] Wang Y C, Wu M Q, Xu F Y and Zhang S R 2005 *The Dielectric Properties of Quartz Glass at High Temperature* Natural Science Edition (J. Sichuan Univ.) vol 42 pp 387–92
[30] Ye J, Wang H and Yang W 2014 Characterization of electrical capacitance tomography sensors with different diameter *IEEE Sensors J.* **14** 2240–51
[31] Girimonte R and Formisani B 2009 The minimum bubbling velocity of fluidised beds operating at high temperature *Powder Technol.* **189** 74–81